International Journal of Thermophysics, Vol. 21, No. 3, 2000

Diffusion Modes of an Equimolar Methane–Ethane Mixture from Dynamic Light Scattering

A. P. Fröba,[1] S. Will,[1,2] and A. Leipertz[1,3]

Received March 30, 1999

The hydrodynamic diffusion modes of an equimolar methane–ethane mixture have been investigated by dynamic light scattering. Measurements were performed over a wide temperature range between the plait critical point at 263.55 K and 310 K along the critical isochore. Two relaxation modes have been observed which are commonly associated with pure mass diffusion and pure thermal diffusion, but in near-critical binary fluid mixtures—according to recent theory—may alternatively be interpreted as two effective diffusivities resulting from a coupling between mass and thermal diffusion. Diffusivity values for the slow mode were obtained with typical standard deviations of 1% over the whole temperature range, whereas the low amplitude of the fast mode only allowed values of this component with a large measurement uncertainty. The results are discussed in connection with literature data available for the thermophysical properties of this binary fluid mixture and regarding the various possibilities of theoretical interpretation.

KEY WORDS: diffusivity; dynamic light scattering; mass diffusion; methane–ethane mixture; near-critical; thermal diffusion.

1. INTRODUCTION

Dynamic light scattering (DLS) is a very useful technique for the determination of transport and other thermophysical properties of fluids and fluid mixtures [1–4]. In pure fluids, the thermal diffusivity can be determined from the linewidth of the Rayleigh component of the spectrum of scattered light, which arises from entropy fluctuations [5–7]. In binary fluid mixtures,

[1] Lehrstuhl für Technische Thermodynamik (LTT), Universität Erlangen-Nürnberg, Am Weichselgarten 8, D-91058 Erlangen, Germany.

[2] Present address: Technische Thermodynamik/Wärme- und Stofftransport, Universität Bremen, FB 4, Badgasteiner Straße 1, D-28359 Bremen, Germany.

[3] To whom correspondence should be addressed.

0195-928X/00/0500-0603$18.00/0

one can basically simultaneously determine the mutual diffusivity and the thermal diffusivity from the linewidth of the Rayleigh line, governed by microscopic fluctuations of temperature and concentration [8–13]. Additionally, for pure fluids as well as for fluid mixtures, information about sound velocity and sound attenuation can be obtained from the Brillouin lines of the spectrum shifted in frequency, which are caused by pressure fluctuations [14–16].

There are many investigations by dynamic light scattering which study the critical behavior of the thermophysical properties of pure fluids and fluid mixtures, e.g., Refs. 17–29. In this context, transport properties are of special interest, e.g., the thermal diffusivity a, mass diffusivity D, and dynamic viscosity η. For pure fluids, it is well known that in the vicinity of the critical point the thermal diffusivity tends to vanish, which has been confirmed by many investigators; see, e.g., Refs. 20–22. The situation is reversed in a binary fluid mixture where the thermal diffusivity either remains finite or shows only a weakly divergent behavior when asymptotically approaching the critical point [26, 30, 31]. Here, the mass diffusion coefficient reflects the critical slowing down of the order-parameter fluctuations and vanishes [32]. In binary liquid mixtures near the consolute point (binary liquid–liquid mixture critical point), the behavior of the mutual mass diffusion coefficient has been studied extensively both by dynamic light scattering and by Taylor dispersion [27–29, 33]. In contrast, only a few investigations of the mutual diffusivity have been carried out on binary mixtures near their vapor–liquid critical points [23, 24]. Furthermore, there is only one experimental investigation available which describes the simultaneous determination of the thermal diffusivity and mutual diffusivity near the plait critical point (binary mixture liquid–vapor critical point) using a binary fluid mixture consisting of 71.07 mol% methane and 28.93 mol% ethane [25].

In this work, we carried out an analysis of the Rayleigh line of an equimolar methane–ethane mixture by dynamic light scattering over a wide temperature range down to the vicinity of the plait critical point. The investigation was initiated by recent research activities of the IUPAC Subcommittee on Transport Properties, which aim at a comprehensive understanding of the transport properties of fluid mixtures in the extended vicinity of the critical point, where an equimolar methane–ethane mixture has been selected as the system for investigation. However, from the lack of reference data for the mutual diffusivity and thermal diffusivity or other properties from which both quantities may be derived, the need for experimental investigations on this equimolar fluid mixture was established. Additionally, experimental data are useful for the corroboration of a recent theory [34], which predicts that in near-critical binary fluid mixtures, the

actually observed phenomena by dynamic light scattering are associated with neither pure mass diffusion nor pure thermal diffusion, but with two effective diffusivities.

2. METHOD

The principles of dynamic light scattering for the determination of transport and other thermophysical properties are described in detail elsewhere [1, 2, 35, 36]. Here, only a few essential features are presented and some relevant aspects of a new interpretation of dynamic light scattering experiments in near-critical binary fluid mixtures, which have been discussed recently in the literature [34], are highlighted.

The relaxation of the two hydrodynamic modes present in binary fluid mixtures follows the same laws which are valid for macroscopic systems. Thus, the decay of temperature and concentration fluctuations is governed by the thermal diffusivity and mutual diffusivity, respectively. Information about these equilibration processes can be derived by the temporal analysis of the scattered light intensity using dynamic light scattering (or photon correlation spectroscopy; PCS). The mean relaxation times of the two hydrodynamic modes are analyzed by the calculation of the time-dependent correlation function of the intensity of scattered light. Taking into account that in a realistic experimental situation, reference light, e.g., stray light from the windows of the measuring cell, is superimposed coherently on the scattered light from the sample, the intensity correlation function takes the form

$$G^{(2)}(\tau) = \underbrace{(I_{LO} + I_t + I_c)^2}_{\text{background}} + \underbrace{2I_{LO}I_t \exp(-\tau/\tau_{C_t}) + 2I_{LO}I_c \exp(-\tau/\tau_{C_c})}_{\text{heterodyne term}} + \underbrace{I_t^2 \exp(-2\tau/\tau_{C_t}) + I_c^2 \exp(-2\tau/\tau_{C_c})}_{\text{homodyne term}} + \underbrace{2I_tI_c \exp(-\tau/\tau_{C_t} - \tau/\tau_{C_c})}_{\text{cross term}} \tag{1}$$

Here, I_{LO} is the intensity of the reference light or the so-called local oscillator, and I_t and I_c denote the scattering light intensities caused by temperature and concentration fluctuations, respectively. In contrast to the homodyne term and cross term, which are due to the scattered light from the sample alone, the heterodyne term is the result of the interference of the scattered and the reference signals. This term is characterized by decay times, τ_{C_t} and τ_{C_c}, which are twice as large as the decay times of the respective homodyne term. The decay time τ_{C_t}, which is equivalent to the mean

lifetime of the temperature fluctuations observed, is related to the thermal diffusivity a by

$$a = \frac{1}{\tau_{C_t} q^2} \tag{2}$$

Equally, from the characteristic decay time τ_{C_c}, which is equivalent to the mean lifetime of the concentration fluctuation observed, the mutual diffusivity D can be determined by

$$D = \frac{1}{\tau_{C_c} q^2} \tag{3}$$

In Eqs. (2) and (3), q is the modulus of the scattering vector,

$$q = |\vec{k}_i - \vec{k}_s| \cong 2k_i \sin(\theta_s/2) = \frac{4\pi n}{\lambda_0} \sin(\theta_s/2) \tag{4}$$

which is defined by the difference of the wave vectors of incident and scattered light, $\vec{k}_i$ and $\vec{k}_s$, respectively. Assuming elastic scattering ($k_i \cong k_s$), the modulus of the scattering vector is given in terms of the fluid refractive index n, the laser wavelength in vacuo λ_0, and the scattering angle θ_s.

Due to the large number of parameters in the correlation function, Eq. (1), it is very difficult to obtain information about the decay times τ_{C_t} and τ_{C_c}. The problem is simplified if heterodyne conditions can be arranged, i.e., $I_t \ll I_{LO}$ and $I_c \ll I_{LO}$. The correlation function is reduced to a sum of two exponentials according to

$$G^{(2)}(\tau) = A + B \exp(-\tau/\tau_{C_t}) + C \exp(-\tau/\tau_{C_c}) \tag{5}$$

where the experimental constants A, B, and C include both the corresponding terms from Eq. (1) and effects that are due to the imperfect signal collection due to the incoherent background and the finite detector area.

Since the mutual diffusivity is, in general, one order of magnitude lower than the thermal diffusivity, the two hydrodynamic modes present in binary fluid mixtures should be observable on different time scales. Whether it is possible to resolve both signals of the correlation function given by Eq. (5) is restricted mainly by the ratio of the scattering intensities I_c/I_t, which depends on the relative difference of the refraction indices of the two components and their concentration. Generally, it is easier to determine both signals in binary mixtures simultaneously if the refractive indices of the two components have comparable values than in the case of

a large difference, where the scattering intensity from concentration fluctuations dominates the correlation function.

A feature that makes dynamic light scattering experiments more complicated is that in near-critical binary fluid mixtures, the physical meaning of the observable quantities may change. The actual observation in near-critical binary fluid mixtures by dynamic light scattering may thus neither be associated with pure mass diffusion nor pure thermal diffusion, but with two effective diffusivities. The reason for this is found in a possible coupling between mass diffusion and thermal diffusion. The two effective diffusvities, D_1 and D_2, or the corresponding decay times, τ_{C_1} and τ_{C_2}, respectively, which can be observed in near-critical binary fluid mixtures by dynamic light scattering, are given by [34]

$$D_{1,2} = \frac{1}{\tau_{C_{1,2}} q^2} = \frac{1}{2}[a + D(1+\kappa)] \mp \frac{1}{2}\sqrt{[a + D(1+\kappa)]^2 - 4aD} \tag{6}$$

The coupling parameter κ, which represents the strength of the coupling between mass and thermal diffusion, is described by

$$\kappa = \frac{k_T^2}{TC_{P,c}} \left(\frac{\partial \mu}{\partial c}\right)_{P,T} \tag{7}$$

where T is the temperature, k_T is the thermal diffusion ratio, $C_{P,c}$ is the isobaric specific heat capacity, μ is the difference between the chemical potentials per unit mass of the two components in the mixture, and c is the mass fraction of the solute. If the coupling between the two hydrodynamic modes is absent ($\kappa = 0$), Eq. (6) reduces to Eq. (2) or (3), and the two effective diffusvities, D_1 and D_2, are associated with the pure mutual diffusivity D and pure thermal diffusivity a, respectively.

3. EXPERIMENTAL

The equimolar methane–ethane mixture investigated in this work was supplied by Praxair with a certified absolute uncertainty in the mole fractions of 0.02 %. Impurities of the mixture were specified as less than 100 ppm. The sample was available in a cylinder of three liters with a pressure of about 40 bar at room temperature, where it was in the one-phase region.

The investigations of the equimolar methane–ethane mixture were performed on the critical isochore ($\rho_c = 8.527\ \text{mol} \cdot \text{L}^{-1}$) over a temperature range from 310 K down to the vicinity of the plait critical point ($T_c = 263.551$ K, $P_c = 67.96$ bar), where the critical data were calculated from the

crossover equation of state of Povodyrev et al. [37]. First, the complete pressure system (see Fig. 1) was filled at room temperature with the help of a gas compressor, resulting in a pressure of about 100 bar. The measuring cell of cylindrical shape (volume, $\approx 10\,\mathrm{cm}^3$) was made of aluminium with two optical accesses, equipped with quartz windows (Herasil I; diameter, 30×30 mm). Due to a small leakage of the sample cell, particularly with variation of the temperature, it was necessary to connect the measuring cell with a reservoir in the form of an expansion bellows by a capillary to maintain the sample on the critical isochore. A coarse adjustment of the pressure, which corresponds to the fixed critical density at any given temperature in the measuring cell, was carried out with the help of a screw press. For a fine adjustment as well as for stabilization during the experiment, a pressure control loop was used consisting of a pressure transducer and resistance heating, which was attached to the expansion bellows. During a single experimental run, the stability of the pressure in the sample cell was better than the resolution of 10 mbar of the pressure transducer, whose absolute measurement accuracy was ± 80 mbar.

The actual temperature in the sample cell, which was placed in a multistage thermostat with a long-term stability better than 2 mK, was regulated through resistance heating. The temperature of the sample was measured with three calibrated 25-Ω platinum resistance probes, integrated into the main body of the measuring cell, with a resolution of 0.1 mK using an AC

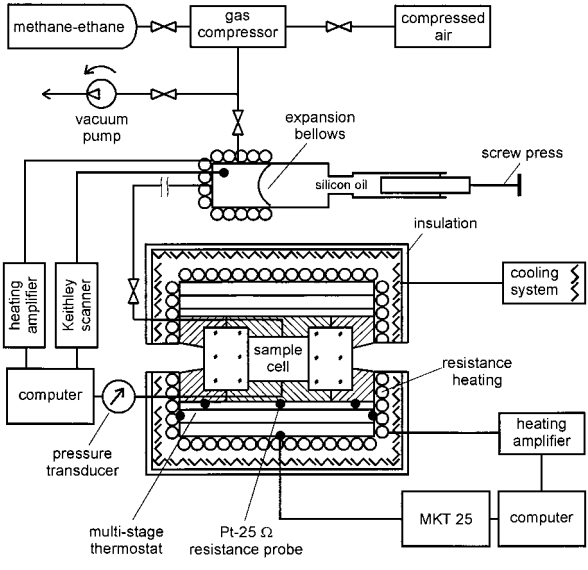

Fig. 1. Experimental setup: pressure and temperature control.

bridge (Paar; MKT 25). The accuracy of the absolute temperature measurement was better than ± 15 mK. For temperatures below room temperature, the insulating house was cooled about 10 K below the desired temperature in the sample cell by a lab thermostat. Due to the difference from ambient temperature and the necessity for optical access, a temperature gradient within the measuring cell could not be completely avoided, but it was less than 3 mK over a distance of about 5 cm from the outer surface of the quartz windows to the middle of the sample. An effect on the measured quantities by the temperature gradient can probably be neglected for the temperature range studied, which is outside of the immediate critical region.

The optical and electronic arrangement of the experimental setup used in this work is shown in Fig. 2. Light from an argon ion laser operating in a single longitudinal mode at 488 nm is directed through a quartz window. The laser power was up to 150 mW when working far from the critical point and only a few milliwatts in the critical region. The system is aligned so that the irradiating focused beam and the axis of observation, which is given by two circular stops with diameters of 1 mm and separated by a distance of about 4 m, intersect in the middle of the sample. Outside the critical region, it turned out that with the small scattering angles ($\theta_s \sim 2.5$–$3°$) used in this work, enough light is scattered at the cell windows to ensure a sufficiently high degree of heterodyning. In the case of high scattering intensities from the sample, an additional reference beam is added. For this, part of the incident beam is reflected by a beam splitter and superimposed on the scattered light behind the sample cell.

With the help of Snell's refraction law and simple trigonometric identities, it can be shown that for small angles, the scattering vector q can be deduced from the angle of incidence θ_i, which is defined (see Fig. 2) as the angle between the optical axis of the incident laser beam and the detection direction:

$$q \cong \frac{2\pi}{\lambda_0} \sin(\theta_i) \tag{8}$$

Equation (8) represents a good approximation for the determination of the scattering vector without the knowledge of the refractive index n of the sample, where the error in q is below 0.04 % for scattering angles up to 3°. For measurement of the angle of incidence, first, the laser beam is adjusted through the detection system, then the laser beam is set to the desired angle. The actual angle of incidence is measured by back reflection from a mirror mounted to a precision rotation table placed on top of the sample cell. The error in the angle measurement has been determined to be

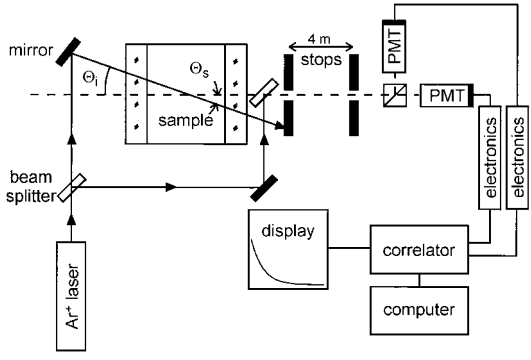

Fig. 2. Experimental setup: optical and electronic arrangement.

approximately $\pm 0.014°$, which results in a maximum uncertainty of less than 1.0% for the diffusivities with a minimum incident angle of 3.5°. For each temperature point, typically six measurements at different angles of incidence were performed, where the laser was irradiated from either side with respect to the axis of observation to check for a possible misalignment. The measurement times for a single run were typically of the order of 10 min down to 1 min for the lowest temperatures in this study.

The scattered light is detected by two photomultiplier tubes operated in cross-correlation mode to suppress afterpulsing effects. The signals are amplified, discriminated, and fed to a digital correlator with a multiple-tau structure, which means that the sampling time of a channel is increased with increasing lag time. This offers the possibility of inspecting various time domains of the correlation function simultaneously. The sampling time is redoubled after a block of eight channels, whereas the first 16 channels have a sampling time of 200 ns. Besides the standardization of the correlation function, the correlator also allows the simultaneous measurement of the photon-counting rate, which is of significance for the determination of the weights of the individual correlator channel contents.

4. DATA EVALUATION

The experimental correlation function, Eq. (5), was evaluated for two effective relaxation times τ_{C_1} and τ_{C_2}, allowing for a possible coupling between thermal diffusion and mass diffusion ($\tau_{C_c} \to \tau_{C_1}$, $\tau_{C_t} \to \tau_{C_2}$). Two exponential signals could be observed at separated time scales ($\tau_{C_1} \sim 3$–$15\tau_{C_2}$) with very different amplitudes ($C \sim 20B$–$150B$). The evaluation of the data sets was done in two steps. First, the signal with a longer decay

time and higher amplitude could be resolved from the measured correlation function if a single-exponential fit was performed for an interval starting at about $4\tau_{C_2}$ and ending at $6\tau_{C_1}$. The long delay time for the start of the fit in the determination of τ_{C_1} was required to suppress completely possible interference from the fast-decaying function. In the second step the correlation function was evaluated by another single-exponential fit at short correlation times ($\tau < \tau_{C_1}$) for the fast mode, after subtracting the result of the first fit for the slow mode. In comparison with a double-exponential fit, the advantage of the described data evaluation procedure is given by the number of free parameters (three) for a single-exponential fit within the relevant fit interval.

The central task of any data evaluation scheme is to check the agreement of the measured data with the theoretical form expected. Thus, a residual plot should be free of any systematic deviations, and the results should be essentially independent of the specific fit interval used. This requirement was fulfilled for the evaluation of the slow mode. There was, however, a systematic deviation of unknown origin for the first correlation channels, which affects the results for the decay time τ_{C_2}. To eliminate possible interference, the first five channels of the experimental correlation functions have been excluded in further evaluation, which may be done

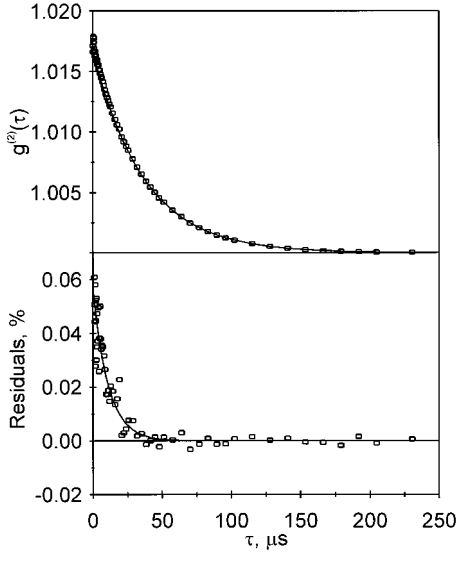

Fig. 3. Fit to an experimental correlation function for the slow mode, and residuals which indicate the presence of a second, faster mode.

without a significant loss of information. With the exception of this short-time interference, no systematic trends have been observed in the data.

In Fig. 3, an example of a fit for the slow mode to an experimental correlation function in standardized form is shown, together with the residuals. From a single-exponential fit to the correlator channels in the time domain $35\,\mu s < \tau < 250\,\mu s$, a decay time τ_{C_1} of $37.10 \pm 0.19\,\mu s$ results. The standard error obtained from the fit may be compared with the deviations obtained from fits to various fit intervals by varying the first channel included in the fit over the range between $0.7\tau_{C_1}$ and $1.1\tau_{C_1}$ and the last channel over a range starting at $2.5\tau_{C_1}$. With this procedure, the standard deviation of these individual fits is 0.8% for τ_{C_1}. Either approach is solely indicative of the uncertainty associated with the determination of the decay time τ_{C_1} from the correlation function. In the residual plot in Fig. 3, a second faster mode can be observed from the systematic positive deviation of the correlation function from the first fit in the range $0\,\mu s < \tau < 25\,\mu s$. From a further single exponential fit in this time domain, on the basis of the result for the slow mode, a decay time τ_{C_2} of $10.96 \pm 0.82\,\mu s$ results. It is obvious, however, that the error in the determination of the decay time τ_{C_2} is about one order of magnitude larger than that for the decay time τ_{C_1}.

5. RESULTS AND DISCUSSION

The experimental results obtained for the diffusivities D_1 and D_2 of an equimolar methane–ethane mixture on the critical isochore over the temperature range from 265 to 310 K are presented in Table I and in Fig. 4. Here the data for D_1 and D_2 represent the average values of typically six measurements at different angles of incidence. The pressure data listed in Table I were adjusted corresponding to the critical density at the given temperatures and are calculated from the crossover equation of state of Povodyrev et al. [37].

The diffusivity D_1 can be well represented by a sum of a polynomial and an additional term, which explicitly takes into account the critical part, resulting in an equation of the form

$$D_1 = \sum_{i=0}^{3} d_i \left(\frac{T}{K}\right)^i + d_4 \left(\frac{T - T_c}{T_c}\right)^{0.67} \tag{9}$$

where the coefficients are given in Table II and the critical temperature was taken as $T_c = 263.551$ K [37]. This value corresponds to the visual observation of maximum opalescence of the sample at a temperature of 263.55 ± 0.03 K. The root-mean-square deviation of our data from the fit according to Eq. (9) is 0.34% over the whole temperature range. The

Table I. Experimental Values for the Diffusivities D_1 and D_2 of an Equimolar Methane–Ethane Mixture on the Critical Isochore

T (K)	P (bar)	D_1 ($10^{-8}\,m^2 \cdot s^{-1}$)	D_2 ($10^{-8}\,m^2 \cdot s^{-1}$)
310.00	127.29	4.387	14.7
308.00	124.64	4.260	17.2
305.00	120.67	4.093	13.2
303.00	118.02	3.959	15.9
300.00	114.07	3.725	13.2
298.00	111.43	3.571	12.6
295.00	107.49	3.332	11.4
293.00	104.87	3.209	13.7
290.00	100.95	2.969	13.5
287.00	97.05	2.714	12.4
285.00	94.45	2.523	11.2
282.00	90.59	2.270	11.3
280.00	88.03	2.060	11.0
277.00	84.21	1.757	12.3
275.00	81.69	1.557	11.5
272.23	78.22	1.249	10.3
270.41	75.97	1.038	8.9
268.99	74.23	0.8676	10.8
267.86	72.87	0.7301	8.3
266.98	71.81	0.6124	—
266.28	70.98	0.5191	—
265.29	69.82	0.3805	—

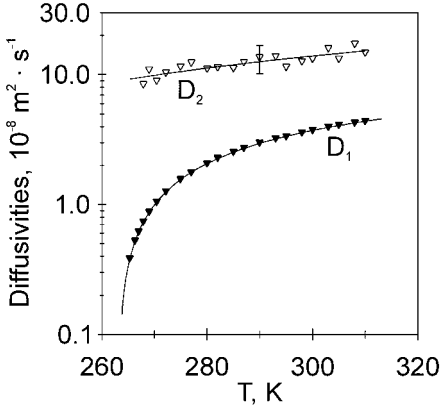

Fig. 4. Measured diffusivities D_1 (▼) and D_2 (▽) for an equimolar methane–ethane mixture along the critical isochore.

standard deviation of our measurements for the diffusivity D_1 is about 1% for temperatures above 290 K and somewhat smaller when approaching the liquid–vapor critical point which results from the increasing signal amplitude for the slow mode with decreasing temperature. Generally, the standard deviation yields an estimate for the absolute accuracy of dynamic light scattering experiments [38]. To check our present data, we carried out two completely independent measurement series at a temperature of 265.29 K, with new samples within the measurement cell and a new adjustment of the optical setup. For the diffusivity D_1, these measurements deviate from each other by only 0.55%.

Due to the low signal amplitude of the fast mode, the diffusivity D_2 could be obtained only with a relatively large measurement uncertainty. The standard deviation of our measurements for the diffusivity D_2 is about 30%. The data indicate a decrease in approaching the liquid–vapor critical point, yet the values for this quantity appear to remain finite. For the temperature range observed, the diffusivity D_2 can be represented by a linear temperature dependence,

$$D_2 = \mathrm{d}_0 + \mathrm{d}_1 \frac{T}{\mathrm{K}} \tag{10}$$

where the constant d_0 and the temperature gradient d_1 are listed in Table II.

In the vicinity of the critical point it has not been possible to perform reasonable light scattering experiments, because there exist some problems in establishing heterodyne conditions by adding an additional reference beam to the scattered light, as shown in Fig. 2. A disturbing signal in the form of an oscillation could be observed in the correlation function. The reason for this interference, which occurred in the same time domain as the slow mode, is still unclear and will be the subject of further investigation. However, down to temperatures $T - T_c > 1.50$ K, heterodyne conditions could be arranged through the stray light from the cell windows alone. Here, the slow mode could be represented well by a simple exponential, indicating the absence of a homodyne term.

Table II. Coefficients of Eqs. (9) and (10)

d_i ($10^{-8}\,\mathrm{m}^2 \cdot \mathrm{s}^{-1}$)	Eq. (9) D_1	Eq. (10) D_2
d_0	−113.3486	−26.5797
d_1	0.9332796	0.135045
d_2	-2.524296×10^{-3}	—
d_3	2.337529×10^{-6}	—
d_4	4.394	—

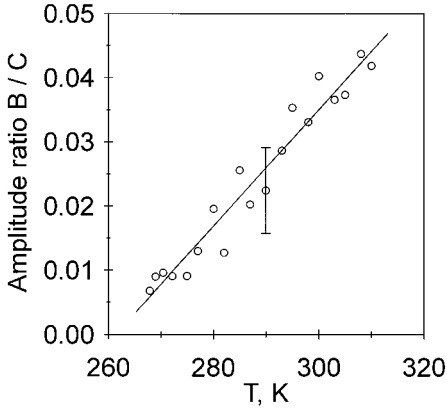

Fig. 5. Measured amplitude ratio of the fast decay signal B to the slow decay signal C for an equimolar methane–ethane mixture along the critical isochore.

Moreover, the data evaluation of the experimental correlation function for the fast mode was limited to temperatures $T - T_c > 4.30$ K. This is due to a decreasing amplitude ratio of the fast decay signal B to the slow decay signal C when approaching the liquid–vapor critical point. Figure 5 shows this behavior of the measured amplitude ratio B/C. Here, the indicated error bar for a single experimental data point represents the standard deviation, which—for the whole temperature range—was between 15% and a maximum of 30% close to the vapor–liquid critical point. Within the measurement accuracy, the behavior of the signal amplitude ratio B/C can be described by a linear function of temperature as depicted by the solid line in Fig. 5.

Finally, our interest is directed to the question of whether the results of the slow mode are coming from pure mass diffusion alone, or if this quantity has to be derived from a combination of D_1 and D_2 because of a coupling between mass and thermal diffusion according to Eq. (6). For this aim, the strength of the coupling parameter κ as described in Eq. (7) may be deduced from a prediction of the thermodiffusion coefficient $k_T D$ and the mutual mass diffusion coefficient D as given in Ref. 39. Furthermore, from this work, values are used for the osmotic susceptibility $(\partial c/\partial \mu)_{P,T}$ and the isobaric specific heat capacity $C_{P,c}$, which are calculated from the crossover equation of state of Povodyrev et al. [37]. In Fig. 6, the dashed line shows the temperature dependence of the estimation of the coupling parameter κ for the temperature range studied. The dotted lines bound the uncertainty intervals, which are calculated from the uncertainty of the

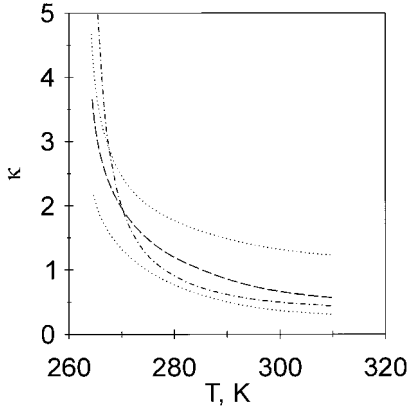

Fig. 6. Estimation of the coupling parameter κ (dashed line), calculated according to Eq. (7) with predicted thermophysical properties given in Ref. 39. The dotted lines bound the uncertainty interval of this estimation. The dotted–dashed line represents the maximum strength of the coupling parameter κ for which a solution of Eq. (6) could be found with the experimental diffusivities D_1 and D_2.

mutual mass diffusion coefficient D and the thermodiffusion coefficient $k_T D$ [39]. Additionally, the dotted–dashed curve in Fig. 6 represents the maximum strength of the coupling parameter κ for which a solution of Eq. (6) could be found with our experimental data. It is clear that on the basis of the uncertainty associated with the calculation of the specific heat capacity $C_{P,c}$ and the osmotic susceptibility $(\partial c/\partial \mu)_{P,T}$ from the crossover equation of state of Povodyrev et al. [37], the resulting uncertainty intervals for the coupling parameter κ must be somewhat larger than depicted by the dotted lines in Fig. 6.

Figure 7 shows the measured diffusivities D_1 and D_2 (solid lines) and the theoretically calculated thermal diffusivity a and mass diffusion coefficient D (dashed lines) according to Eq. (6) based on the estimated coupling parameter κ, as depicted in Fig. 6. A solution for the desired quantities based on our experimental data and the coupling parameter could be found only for the limited temperature range $T < 271$ K. The behavior of the diffusivities a and D is also calculated for the upper and lower limits of the uncertainty interval of the coupling parameter κ and depicted in Fig. 7 (dotted lines). In contrast to the upper limit, a solution for the thermal diffusivity a and the mutual mass diffusion coefficient D based on the lower

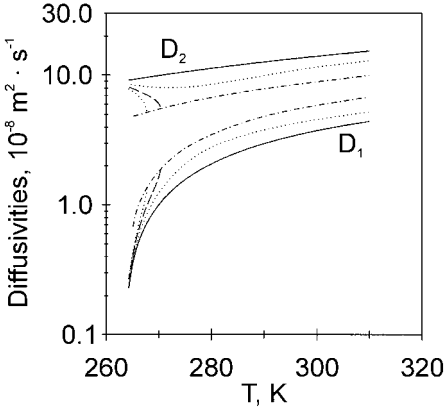

Fig. 7. Measured diffusivities D_1 and D_2 in comparison with theoretically calculated values for the thermal diffusivity a and the mass diffusion coefficient D according to Eq. (6) in the case of a possible coupling between the hydrodynamic relaxation modes. The theoretically calculated values for a and D correspond to the curves for the coupling parameter κ depicted in Fig. 6.

limit could be found for the whole temperature range studied in this work. Furthermore, the dotted–dashed curves in Fig. 7 correspond to the maximum coupling parameter κ for which a solution of Eq. (6) could be found with our experimental data.

For the slow mode, our experimental and theoretically calculated values may be compared with predicted values for the binary diffusion coefficient D from the work of Sakonidou et al. [39]. Figure 8 presents this prediction (dashed line) in comparison with our measured values (solid line) for the slow mode and calculated values (dotted line) in the case of a coupling between thermal and mass diffusion. Here, only the theoretically calculated values for the lower limit of the uncertainty interval of the coupling parameter, as shown in Fig. 6, are shown. The dotted–dashed lines in Fig. 8 indicate the uncertainty interval for the prediction by Sakonidou et al. [39]. Generally, in the case of a coupling between mass and thermal diffusion, according to Eq. (6), the effective diffusivity D_1 observable by dynamic light scattering should be lower than the mass diffusivity D. Yet, in the existing comparison, this relationship is inverted. By this, the discrepancies between our experimental results and the prediction by Sakonidou et al. [39] would become much larger if a coupling between mass and thermal diffusivity should be of significance for dynamic

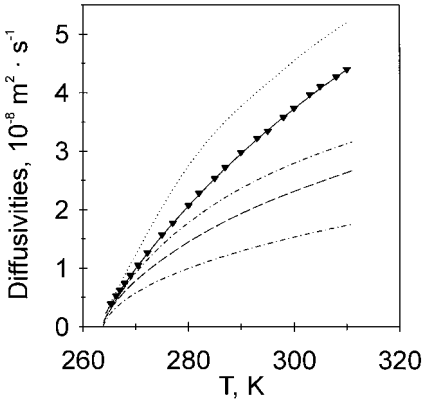

Fig. 8. Measured diffusivity D_1 (▼) and theoretically calculated values for the mutual mass diffusivity D (dotted line) based on the lower limit of the uncertainty interval for the coupling parameter κ (see Fig. 6) in comparison with a prediction for the mass diffusivity D (dashed line) from Ref. 39. The dotted–dashed lines indicate the uncertainty interval of this prediction.

light scattering experiments in near-critical binary mixtures. Due to the large measurement uncertainty for the fast mode, a data comparison of our experimental and theoretically calculated data with reference values for the thermal diffusivity a has not been performed in this work.

6. CONCLUSIONS

We have shown that dynamic light scattering can be applied to measure simultaneously the two hydrodynamic diffusion modes present in binary fluid mixtures. For an equimolar methane–ethane mixture, values for the two diffusivities, which are commonly interpreted as pure mass diffusivity and thermal diffusivity, have been observed over the temperature range from 265 to 310 K. A comparison of the results obtained for the slow mode with predicted data for the binary diffusion coefficient shows discrepancies which are outside the combined uncertainty of our data and of this prediction, which indicates that the predicted values for the binary diffusion coefficient are subject to a much larger uncertainty than stated, especially for temperatures far away from the critical point. Furthermore, in the case that a coupling between mass and thermal diffusivity should play a role for dynamic light scattering experiments in a near-critical binary

fluid mixture, as reported in the literature recently, the discrepancies between the predicted values for the mutual mass diffusivity and our data would become much larger. Due mainly to the uncertainties of the predicted values for the binary diffusion coefficient, however, the question of whether the data for the slow mode are associated with pure mass diffusion or must be interpreted with an effective diffusion mode could not be answered. To give a more accurate prediction for the diffusivites in the case of a possible coupling between mass and thermal diffusion, more accurate values for the thermodiffusion coefficient are necessary which, in addition to the isobaric specific heat capacity and the osmotic susceptibility, define the strength of the coupling. Experimental values for the thermal diffusivity and the mass diffusion coefficient obtained by other techniques may be most helpful in clarifying the question of whether the diffusion modes obtained by dynamic light scattering may be directly associated with a and D also in near-critical binary fluid mixtures. These first experimental data on an equimolar methane–ethane mixture from dynamic light scattering may further stimulate theoretical and experimental investigations in this field.

ACKNOWLEDGMENTS

This work is dedicated to the memory of H. R. van den Berg. The authors are grateful for his helpful cooperation in and valuable contributions to the experimental part of this work. Valuable contributions by M. A. Anisimov in the early stage of this study are gratefully acknowledged. We would also like to thank W. A. Wakeham, V. Vesovic, and E. P. Sakonidou for many valuable discussions concerning the analysis and interpretation of the data. Parts of the work were supported by the Deutsche Forschungsgemeinschaft (DFG).

REFERENCES

1. J. N. Shaumeyer, R. W. Gammon, and J. V. Sengers, in *Measurement of the Transport Properties of Fluids*, W. A. Wakeham, A. Nagashima, and J. V. Sengers, eds. (Blackwell Scientific, Oxford, 1991), pp. 197–213.
2. S. Will and A. Leipertz, in *Diffusion in Condensed Matter*, J. Kärger, P. Heitjans, and R. Haberlandt, eds. (Vieweg, Wiesbaden, 1999), pp. 219–244.
3. A. Leipertz, *Fluid Phase Equil.* **125**:219 (1996).
4. K. Kraft, S. Will, and A. Leipertz, *Measurement* **14**:135 (1994).
5. M. Corti and V. Degiorgio, *J. Phys. C Solid State Phys.* **8**:953 (1975.)
6. M. Hendrix, A. Leipertz, M. Fiebig, and G. Simonsohn, *Int. J. Heat Mass Transfer* **30**:333 (1987).
7. S. Will, A. P. Fröba, and A. Leipertz, *Int. J. Thermophys.* **19**:403 (1998).
8. C. J. Coumou and E. L. Mackor, *Trans. Faraday Soc.* **60**:1726 (1964).
9. R. D. Mountain and J. M. Deutch, *J. Chem. Phys.* **50**:1103 (1969).

10. P. Berge, P. Calmettes, M. Dubois, and C. Laj, *Phys. Rev. Lett.* **24**:89 (1970).
11. E. Gulari, R. J. Brown, and C. J. Pings, *AIChE J.* **19**:1196 (1973).
12. G. Wu, M. Fiebig, and A. Leipertz, *Int. J. Heat Mass Transfer* **31**:2555 (1988).
13. H.-W. Fiedel, G. Schweiger, and K. Lucas, *J. Chem. Eng. Data* **36**:169 (1991).
14. G. Simonsohn, *Opt. Acta* **30**:875 (1983).
15. A. Leipertz, K. Kraft, and G. Simonsohn, *Fluid Phase Equil.* **79**:201 (1992).
16. K. Kraft and A. Leipertz, *Int. J. Thermophys.* **16**:445 (1995).
17. M. A. Anisimov, *Critical Phenomena in Liquids and Liquid Crystals* (Gordon and Breach, Philadelphia, 1991).
18. R. W. Gammon, H. L. Swinney, and H. Z. Cummins, *Phys. Rev. Lett.* **19**:1467 (1967).
19. G. Simonsohn and F. Wagner, *J. Phys. D Appl. Phys.* **24**:415 (1991).
20. T. Kun Lim, L. Swinney, K. H. Langley, and A. Kachnowski, *Phys. Rev. Lett.* **27**:1776 (1971).
21. B. J. Ackerson and G. C. Straty, *J. Chem. Phys.* **69**:1207(1978).
22. P. Jany and J. Straub, *Int. J. Thermophys.* **8**:156 (1987).
23. D. L. Henry, L. E. Evans, and R. Kobayashi, *J. Chem. Phys.* **66**:1802 (1977).
24. Y. Miura, H. Meyer, and A. Ikushimak, *J. Low Temp. Phys.* **55**:247 (1984).
25. B. J. Ackerson and H. J. M. Hanley, *J. Chem. Phys.* **73**:3568 (1980).
26. P. Calmettes and C. Laj, *Phys. Rev. Lett.* **36**:1372 (1976).
27. H. L. Swinney and D. L. Henry, *Phys. Rev. A* **8**:2586 (1973).
28. G. Wu, M. Fiebig, and A. Leipertz, *Wärme-Stoffübertr.* **22**:365 (1988).
29. S. Will and A. Leipertz, *Int. J. Thermophys.* **20**:791 (1999).
30. M. A. Anisimov, E. E. Gorodetskii, V. D. Kulikov, A. A. Povodyrev, and J. V. Sengers, *Physica A* **220**:277 (1995); *Physica A* **223**:272 (1996).
31. M. A. Anisimov, E. E. Gorodetskii, V. D. Kulikov, and J. V. Sengers, *Phys. Rev. E* **51**:1199 (1995).
32. L. Mistura, *Nuovo Cimento B* **12**:35 (1972).
33. M. L. S. Matos Lopes, C. A. Nieto de Castro, and J. V. Sengers, *Int. J. Thermophys.* **13**:283 (1992).
34. M. A. Anisimov, V. A. Agayan, A. A. Povodyrev, J. V. Sengers, and E. E. Gorodetskii, *Phys. Rev. E* **57**:1946 (1998).
35. B. Chu, *Laser Light Scattering*, 2nd ed. (Academic Press, New York, 1991).
36. B. J. Berne and R. Pecora, *Dynamic Light Scattering* (Wiley-Interscience, New York, 1976).
37. A. A. Povodyrev, G. X. Jin, S. B. Kiselev, and J. V. Sengers, *Int. J. Thermophys.* **17**:909 (1996).
38. K. Kraft, M. Matos Lopes, and A. Leipertz, *Int. J. Thermophys.* **16**:423 (1995).
39. E. P. Sakonidou, H. R. van den Berg, and C. A. ten Seldam, *J. Chem. Phys.* **109**:717 (1998).